Pharm Res (2015) 32:3309–3323
DOI 10.1007/s11095-015-1708-0

RESEARCH PAPER

Stealth Nanogels of Histinylated Poly Ethyleneimine for Sustained Delivery of Methotrexate in Collagen-Induced Arthritis Model

SamiraSadat Abolmaali[1] • AliMohammad Tamaddon[1] • Eskandar Kamali-Sarvestani[2] • MohammadJavad Ashraf[3] • Rasoul Dinarvand[4]

Received: 16 January 2015 / Accepted: 5 May 2015 / Published online: 12 May 2015

ABSTRACT

Purpose The study aimed to illustrate application of polycation Stealth nanogels for sustained delivery of methotrexate (MTX) in collagen induced arthritis (CIA) model in C57Bl/6 mice.

Methods Nanogel synthesis involves metal ion coordinated self-assembly of PEGylated poly ethyleneimine (L-histidine substituted), chemical crosslinking and subsequent removal of the coordinated metal. The nanogels were characterized by TEM and DLS-zeta potential. Comparative efficacy and pharmacokinetics of the i.v. administred MTX-loaded nanogels were investigated in the CIA model. Inflammation site passive accumulation of the fluorophore-labeled nanogels was tested using *in-vivo* imaging of mice paw received unilateral injection of lipopolysaccharide.

Results Uniform nanogels (sizes ~40 nm by TEM) were loaded with MTX (entrapment efficiency = 62% and drug loading = 54% at the MTX feeding ratio of 0.3 relative to total molar concentration of the polymer amines). The nanogels exhibited neutral surface charge and an acceptable biocompatibility in terms of albumin aggregation, hemolysis, erythrocyte aggregation and cytotoxicity. Single dose pharmacokinetics of the MTX-loaded nanogels, unlike free drug, showed a sustained plasma profile. When arthritis established as confirmed by histopathology, a remarkable decline of paw swelling and clinical scores was observed. Fluorescence intensity of the nanogels was enhanced about 2.7 folds at the inflamed than control normal ankle.

Conclusion Sustained delivery of MTX and preferential accumulation of the nanogels in inflamed paw might explain the superior clinical outcome of the MTX-loaded nanogels.

KEY WORDS clinical efficacy · collagen induced arthritis · methotrexate · pharmacokinetics · stealth nanogels

Electronic supplementary material The online version of this article (doi:10.1007/s11095-015-1708-0) contains supplementary material, which is available to authorized users.

✉ AliMohammad Tamaddon
amtamadon@gmail.com; amtamadon@sums.ac.ir

SamiraSadat Abolmaali
s.abolmaali@gmail.com

Eskandar Kamali-Sarvestani
immunol2@gmail.com

MohammadJavad Ashraf
Ashrafm@sums.ac.ir

Rasoul Dinarvand
dinarvand@tums.ac.ir

[1] Center for Nanotechnology in Drug Delivery, Department of Pharmaceutical Nanotechnology, Shiraz University of Medical Sciences, Shiraz 71345, Iran

[2] Autoimmune Diseases Research Center and School of Medicine Department of Immunology, Shiraz University of Medical Sciences, Shiraz 71345, Iran

[3] Department of Pathology, School of Medicine, Shiraz University of Medical Sciences, Shiraz 71345, Iran

[4] Nanotechnology Research Centre and Faculty of Pharmacy, Tehran University of Medical Sciences, Tehran 14174, Iran

ABBREVIATIONS

CFA	Complete Freund's adjuvant
CIA	Collagen induced arthritis
CR	Molar ratio of the crosslink (DTDP) to NH2
FR	Molar ratio of methotrexate to total amines
H-PEI	Histidinylated poly ethyleneimine
HP-PEI	PEGylated poly ethyleneimine (L-histidine substituted)
MRT	Mean residence time
MTX	Methotrexate
PDI	Polydispersity index
P-PEI	PEGylated poly ethyleneimine
RA	Rheumatoid arthritis
Vss	Apparent volume of distribution at steady state

INTRODUCTION

Rheumatoid arthritis (RA) is a severe immune-mediated disease characterized by chronically progressive inflammation and destruction of joints and associated structures. Since there is no cure for rheumatoid arthritis, the therapeutic goals are remission of symptoms involving the joints with steroidal and non-steroidal anti-inflammatory drugs and maintenance of the remission with disease-modifying anti-rheumatic drugs (1). Methotrexate (2, 4-diamino-N10-methyl propylglutamic acid or MTX) is one of the most widely studied and effective therapeutics agents available to treat many solid tumors, hematologic malignancies and autoimmune diseases (2). Application of low-dose MTX in treatment of RA was approved by Food and Drug Administration in 1988 and now is considered as gold standard therapy (3).

There are some limitations for efficient MTX therapy in RA. Pharmacokinetics of MTX is unsatisfactory and may result in inadequate clinical response. Large amounts of the administered dose are eliminated by the kidneys within a short period of time, resulting in short plasma half-life of 5–8 h in human and a low drug concentration in the target tissues. Increasing the dose may result in a higher therapeutic efficacy but leads to a higher risk of side effects. General toxicities leads to discontinuation of MTX therapy in approximately 30% of RA patients (4).

To improve the poor pharmacokinetic of MTX, nanotechnology based delivery systems are developed. Such systems exploit unique pathophysiological features of inflamed joints which has been recently reviewed (5) including porous vasculature and impaired lymphatic drainage well known as enhanced permeability and retention (EPR effect) (6), angiogenesis (7), tissue hypoxia and acidosis (8), expression of specific antigens and receptors (9), and accumulation of inflammatory cells. Thus far, many forms of particulate systems such as human serum albumin (10), liposomes (11) and polymeric microspheres (12) are developed to control the drug disposition and to lower off-target side effects. However, some challenges such as 1) low drug loading capacity, 2) little evidence to support clinical efficacy in RA and 3) low patient compliance for intraaticular injection hamper the utility of these systems regardless of targeting ligands that may have been used. To address some of these challenges, we introduce a nanogel formulation.

Nanogels are in general physically or chemically crosslinked hydrophilic nanostructures that mesh well with extracellular matrices, and thus demonstrate a superior biocompatibility (13), ability to reach the smallest capillary vessels (14) and forced renal filtration through pores even 1/10 of their size (15) due to their mechanical flexibility. Polyelectrolyte nanogels are considered for efficient loading and sustained release of ionizable molecules such as MTX (a weak bicarbocylic acid with pKa of 3.8 and 4.8 and log $P=-0.24$) through diffusion within 3D matrix of the nanogels which contains high water content.

One way to produce polyelectrolyte nanogels is to crosslink transition metal-coordinated micellar templates (5). Coordination of transition metals such as Zn^{2+} with polyelectrolytes leads to formation of the hydrophobic domains, which tend to agglomerate in aqueous media. Conjugation of water soluble polymers, such as poly ethylene glycol (PEG), prevents aggregation and macroscopic phase separation. Subsequently, partial chemical crosslinking and subsequent removal of the metal develop sterically stabilized (Stealth) nanogels with a fairly narrow size distribution. Branched poly ethyleneimine (PEI), a cationic polyelectrolyte, is chosen as the polymer backbone since it contains high quantity of multiple amine groups enable 1) coordination with transition metals (16) and 2) conjugation to PEG to reduce safety problems (17), to avoid interactions with plasma components and rapid uptake by reticuloendothelial system, and consequently to enhance blood longevity (18). Our previous report demonstrates some key structural features of the nanogels for effective MTX delivery (19): 1) efficient microencapsulation of negatively charged molecules such as MTX, 2) crosslink biodegradability which promotes breakdown of the nanogel (20) and 3) superior cytocompatibility if compared to the uncrosslinked polymers.

Considering the several advantages of PEI modification with L-histidine, an alpha amino acid with an imidazole functional group (pKa = 6.1), to induce polymer gelation at a lower critical quantity of transition metals and to further enhance biocompatibility (16), we aimed in the present study to develop L-histidine substituted nanogels and to study their application for sustained delivery of MTX in collagen induced arthritis (CIA) model of RA.

MATERIALS AND METHODS

Materials

Branched poly ethyleneimine 10 kDa (corresponding to Mw/Mn of 1.4) and methoxy poly ethylene glycol 2 kDa

(mPEG2000-COOH) were purchased from Poly Sciences Inc. (Canada) and Jenkem (USA), respectively. Methotrexate (MTX) was obtained from Heumann (Germany). Fmoc protected L- histidine purchased from Bachem (Germany). Freund's complete adjuvant, Collagen type II from chicken sternal cartilage, Killed Mycobacterium tuberculosis H37Ra, Lipopolysaccharide (LPS), Bovine serum albumin, Dithiodipropionic acid (DTDP), 1-(3-dimethylaminopropyl)-3-ethylcarbodiimide hydrochloride (EDC) and N-hydroxysuccinimide (NHS), dicyclohexylcarbodiimide (DIC), disodium ethylenediaminetetraacetic acid (EDTA) and Triton X-100 were supplied by Sigma-Aldrich. ZnSO4.7H2O, piperidine, dichloromethane, perchloric acid, dimethylsulfoxide (DMSO), diethyl ether, triethylamine and 2-Morpholinoethanesulfonic acid (MES) were purchased from Merck (Germany). Deionized water (Direct Q UV3, Millipore, USA) was used for all experiments. Sulfo-cyanine 5.5 NHS ester was obtained from Lumiprobe (USA) for fluorophore labeling of the nanogels.

Coordination-Assisted Synthesis of Nanogels

As shown in Fig. 1, development of nanogels were based on synthesis of PEGylated PEI backbone, formation of Zn^{2+} coordinated micellar template, and consequent crosslinking reaction according to our previously published method (5). In line with superior gelation property of PEI after L-histidine substitution (16), the polymer backbone was first modified with Fmoc-protected L-histidine. Briefly, 190 mg Fmoc α-amino protected L-histidine-COOH was activated with 115 mg NHS and 158 µl DIC in 2 ml of DMSO for 1 h. Then, 1 ml of the above solution was reacted with 2 ml of 1% PEI in DMSO. The reactions were supplemented with 30 µl triethylamine and incubated for 2 h at 25°C. To remove Fmoc, 500 µl of piperidine was added to the reaction tubes and the mixture was further incubated for 20 min. The products were precipitated by cold diethyl ether / acetone (4:1) and were recovered by centrifugation at 3000×g for 30 min. The obtained pale yellowish sediments were reconstituted in deionized water, further purified by Float-A-Lyzer 3.5 KDa (Spectrum, USA) and lyophilized. The average molecular weight (Mn) of histidinylated PEI (H-PEI) was estimated 21.4 kDa by proton integration method using ^{1}H-NMR spectrograms in D_2O (Supplementary Data 1). Moreover, gel filtration chromatography was performed on TSKgel PW5000XL to confirm polymer purification by the dialysis method (Supplementary Data 2).

To 2 ml of 5%*w*/*v* histidinylated PEI (H-PEI) solution in dichloromethane, 1 ml of 5%*w*/*v* methanolic solution of NHS-activated $mPEG_{2000}$-COOH was added to obtain the nominal weight fraction of PEG = 0.33. The reaction medium was supplemented with 15 µl of TEA under stirring at room temperature. The PEGylated products were concentrated using RVC 2–18 rotational speed-vacuum (Christ, Germany), purified using Float-A-Lyzer 8–10 kDa and lyophilized. The PEGylated L-histidine substituted product (HP-PEI) was characterized by ^{1}H-NMR spectroscopy in D_2O (Supplementary Data 1).

To prepare Zn^{2+}-coordinated micellar template, 100 mM $ZnSO_4$ solution in 100 mM MES buffer (pH = 5, 6.5 or 8) was added to 1% HP-PEI solution in deionized water at different molar ratios of Zn^{2+} to the polymer nitrogen (Zn^{2+}/N = 0.1, 0.4 or 0.7). The mixtures were vigorously micro-pipetted and incubated for 30 min. The crosslinking reaction was achieved *via* condensation happened between the carboxylic groups of 100 mM DTDP solution in DMSO and free amines of Zn^{2+}-coordinated HP-P dispersion using 400 mM EDC and 400 mM NHS. Degree of crosslinking was controlled by the crosslink ratio (CR) defined as the molar ratio of DTDP to primary amines (0.3, 0.6 or 1.2). The reaction mixtures were allowed to stir overnight and subsequently dialyzed against acidic deionized water (pH = 3) using Float-A-Lyzer 6–8 kDa to remove Zn^{2+} from the crosslinked templates. ^{1}H-NMR spectroscopy was performed to estimate crosslink density per primary amines of nanogel that was calculated 7.0 and 10.8% with the nominal crosslink ratio of 0.3 and 0.6, respectively. FTIR spectroscopy was performed to study spectral changes of HP-PEI upon coordination with Zn^{2+}, crosslinking reaction and subsequent removal of Zn^{2+} (Supplementary Data 3).

Methotrexate Loading

An aliquot of 2 mg/ml aqueous dispersion of uncrosslinked polymer or the nanogels (CR of 0.3 or 0.6) was mixed with MTX solution in deionized water (1:1 *v*/*v*) at different feeding ratios (FR) of 0.15, 0.30 and 0.60 mol/mol (MTX : total polymer amines) which correspond to the final MTX concentrations of 2.3, 4.6 and 9.2 mM. Then, pH was adjusted to 6 and the mixture was incubated for 72 h at room temperature while shaking at 400 rpm. Unbound MTX was removed by ultrafiltration using Amicon YM-30 centrifugal filter devices (Millipore, USA). The concentration of MTX in filtrates was determined using HPLC system (Knauer, Germany) equipped with a multiple wavelength UV 2600 detector. Separation of MTX was achieved at ambient temperature using Chromolith monolithic reversed phase column (RP-18e, 5–4.6 mm, Merck, Germany). The mobile phase composed of 100 mM sodium acetate (pH = 4)-acetonitrile (88:12, *v*/*v*) was delivered isocratically at a flow rate of 2 ml/min. Entrapment efficiency (percentage of MTX entrapped to the total amount added), the mass

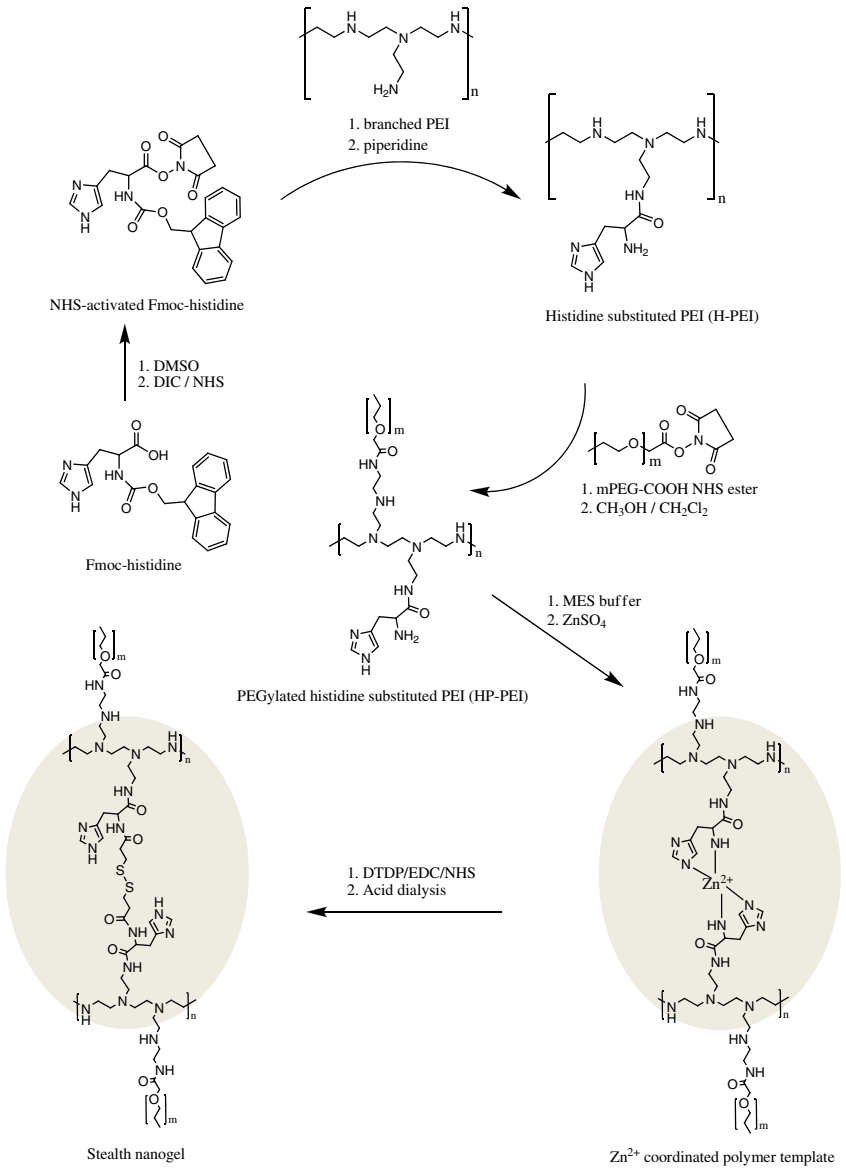

Fig. 1 Schematic route of synthesis of L-histidine-substituted nanogels.

ratio of entrapped MTX to the polymer, and drug loading (weight percentage of the entrapped MTX to the total carrier system) were calculated as a function of FR and CR according to the following equations:

$$Entrapment\ efficiency(EE\%) = \left\{1 - \frac{MTX\ concentration\ in\ filtrate}{feeding\ concentration\ of\ MTX}\right\} \times 100$$

$$Mass\ ratio\ (entrapped\ MTX/polymer\ ,\ w/w) = \frac{EE\%\ \times\ feeding\ concentration\ of\ MTX(\mu M) \times\ M.W._{.\,MTX}}{Polymer\ concentration(mg/ml)\ \times 10^4}$$

$$Drug\ loading(\%)\ =\ \left\{\frac{Mass\ ratio}{1 +\ Mass\ ratio}\right\} \times 100$$

Dynamic Light Scattering and Zeta-Potential

The intensity averaged hydrodynamic diameter (Z-average) and polydispersity index (PDI) of Zn^{2+}-coordinated micelles and the nanogels before and after loading MTX were determined by dynamic light scattering (Zetasizer 3000HSA, Malvern Instruments, UK). Zeta-potential measurements were performed in phosphate buffered saline (PBS, 10 mM phosphate + 140 mM NaCl, pH = 7.4).

Transmission Electron Microscopy

Sample preparation for transmission electron microscopy (TEM) was carried out based on the published method (21). Briefly, a drop of nanogel was allowed to settle on copper grid for 1 min. Excess sample was wicked away with filter paper,

and a drop of 1% uranyl acetate solution was allowed to contact the sample for 20s. The samples were air-dried and studied using a Zeiss EM 10C transmission electron microscope at 80 kV.

In-Vitro Drug Release

Release of MTX from the loaded nanogels was investigated in 25 mM phosphate buffer (pH 7.4) containing 140 mM NaCl or 5% dextrose. Briefly, 4 mL of the MTX-loaded nanogels or free MTX (the corresponding concentration of 0.77 mM) was placed in Float-A-Lyzer 8–10 kDa and dialyzed against 400 mL of the release media in shaker incubator at 37^0C and 100 rpm. At scheduled times, 1 ml of the release medium was withdrawn and concentration of the released drug was determined by the HPLC method as described before. The first 60% of drug release data were fitted to different mathematical functions (zero-order, first-order, Higuchi and Korsmeyer-Peppas) using nonlinear regression. The Korsmeyer-Peppas equation (22) was selected ($r^2 > 0.99$) and accordingly the release rate constant (k) and the release exponent (n) were calculated.

Hemocompatibility

Hemocompatibility of the nanogels were investigated in terms of hemolysis, erythrocyte and human serum albumin aggregation assays in comparison to uncrosslinked HP-PEI and PEI. The hemolytic activity was studied according to the published method (23). Briefly, blood was collected from anaesthetized Wistar rats by cardiac puncture according to the standard operation procedure. Following centrifugation at 700×g for 10 min, the pellet was washed with cold PBS (pH=7.4). To 1 volume of the erythrocytes, 10 volumes of the polymers were rapidly added and mixed in a Revolver Rotator (Labnet, USA) for 60 min at 37°C. Hemoglobin release (%) was determined after centrifugation at 5000×g for 15 min by spectrophotometric analysis of the supernatant at λ=540 nm *versus* complete lysis achieved with 0.2% Triton X-100. To assay erythrocyte aggregation, samples were immediately imaged following incubation with the polymer solutions using an inverted-light microscope (Optika, Italy) at 200× magnification. The images were scored for the size of erythrocyte aggregates as previously described (24).

To assay albumin aggregations induced by the polymers, different volumes of 20 mg/ml solution of human serum albumin (2, 5 or 10 µl) were added to 100 µl of 1 mg/ml solution of the polymers. Then, the mixture was shaken for 30s and allowed to stand for 10 min. The optical density of each solution was measured at λ=420 nm and then transformed to turbidity.

Animals

Seven to Nine week old female in-bred C57Bl/6 mice weighing 19–21 g were provided by Pasteur Institute (Tehran, Iran). Mice were kept under the standard housing conditions and had access to standard chow and water *ad libitum*. All experiments were performed according to Code of Ethics and Practice approved by the animal subject review committee and humane care of the animals with animal studies, Shiraz University of Medical Sciences. .

Methotrexate Pharmacokinetics

Thirty six mice were randomly allocated into two groups. Serial sacrifice design was used to compare single-dose pharmacokinetic parameters of MTX solution (Group 1) to MTX-loaded nanogel (Group 2). The mice were intravenously injected within 1 min from the tail vein with 100 µl aliquot of 7 mg/kg MTX. At different time intervals, blood was collected from anaesthetized mice ($n=3$) by cardiac puncture. Following centrifugation at 2000×g for 15 min at 4°C, 10 µl of 60 mg/ml timolol (internal standard) was added to 390 µl aliquot of the supernatant. Then, the samples were supplemented with 100 µl of 70% perchloric acid and mixed by a vortex for 30s. They were maintained for 15 min and centrifuged at 3000×g for 10 min. Then, the samples were injected into the validated HPLC system for determination of MTX concentration in plasma (Supplementary Data 4). Area under the plasma concentration-time curve from time zero to 120 min (AUC_{0-t}) and from zero to time infinity ($AUC_{0-\infty}$) were calculated by the partial AUC method. Also, Areas under the moment curve ($AUMC_{0-t}$ and $AUMC_{0-\infty}$), total body clearance (Cl), the mean residence time (MRT), the effective half-life ($t_{1/2}$) and the apparent volume of distribution at steady state (V_{ss}) were calculated (Supplementary Data 5) (25).

Collagen-Induced Arthritis Model

Collagen-induced arthritis was developed in C57Bl/6 mice according to the protocol described by Bevaart *et al.*(26). Briefly, 5 mg lyophilized chicken type II collagen, from chicken sternal cartilage, was dissolved in 2.5 ml of 0.1 M acetic acid overnight at 4°C. The collagen solution was emulsified on ice with 5 mg/ml complete Freund's adjuvant (CFA) using a mechanical homogenizer. Mice were anesthetized by intraperitoneal administration of 90 mg/kg ketamine and 10 mg/kg xylazine. Using a glass syringe and 25G needles, 0.1 ml of emulsion was injected intra-dermally into the base tail of mice. This volume was divided over two injection sites. On Day 21 after the first injection, mice were injected again intra-dermally at the base of tail close to previous injection sites with a chicken type II collagen/CFA emulsion. The

control mice were received only normal saline injections scheduled at the same times.

Arthritis was monitored by measuring the mouse weight using an analytical balance and the paw swelling by a digital calliper every other day until Day 33. The mice were scored using a clinical arthritis scoring system that measures the outward symptoms as follows: 0 (no inflammation or normal); 1 (mild erythema and swelling of one joint); 2 (moderate erythema and swelling of two joints or more); 3 (severe erythema and swelling of the entire paw); 4 (joint distortion and /or rigidity and dysfunction) (26). Paw swelling was recognized if the paw diameter was significantly above the baseline values. All measurements and the scoring started 1 week before the booster injection for baseline measurements of non-inflamed joints and mouse weight.

Treatment Protocol and Clinical Evaluation

Twenty C57Bl/6 mice manifested the clinical score of at least 2 were distributed randomly among treatment and control groups on Day 26. Each group ($n=5$) received a volume of 100 µl injection intravenously each day for 1 week:

Group 1	Received 1 mg/kg/day of free MTX solution
Group 2	Received 1 mg/kg/day of MTX as loaded nanogel dispersion (equivalent to 0.8 mg polymer/kg/day)
Group 3	Received 0.8 mg /kg/day empty nanogel dispersion
Group 4 (control)	Received normal saline

The relative changes in mouse weight, paw swelling and the clinical score were considered with respect to the baseline value on Day 21. The mice were inspected daily for possible side effects associated with the treatments.

Histopathological Evaluation

The CIA mice received MTX-loaded nanogel or normal saline according to the treatment protocol were sacrificed on Day 33. The paws were isolated and fixed with % formalin. After 1 week, the paws were transferred into 0.5 M EDTA decalcification solution. After 4 weeks, the paws were paraffin-embedded and 5 µm sagittal sections of whole paws were made. The sections were transferred onto glass slides and stained with hematoxylin and eosin for light microscopy evaluation.

In-Vivo Fluorescent Imaging

To visualize passive accumulation of HP-PEI nanogels in the inflamed mice paw, LPS-induced arthritis was developed in C57Bl/6 mice according to the published method (27). The mice received a 20 µl intra-articular injection of 0.5 mg/ml LPS solubilized in normal saline into the left ankle joint through the Achilles tendon using a 30-gauge needle. As a control, the same volume of normal saline was injected into right ankle joint of the same animal. One day after induction, mice were anesthetized with intra-peritoneal injection of 90 mg/kg ketamine and 10 mg/kg xylazine. Then, the mice ($n=5$) received intravenously a volume of 100 µl of the sulfocyanine 5.5 NHS ester conjugated nanogels (0.21 mg/kg). The mice paw was imaged using Kodak FPRO *in-vivo* imaging system (Rochester, NY, USA) after 30 min, 1 h and 4 h (excitation filter = 630 nm, emission filter = 750 nm, field of view = 60 mm, f-stop = 2.8 and exposure time = 30 s). Background and fluorescent images were analyzed using commercially available software Digital Science 1D software (Kodak, Rochester, NY, USA). The images with normalized dynamic range were merged with built-in image Math Option. Then, the signal intensities were re-scaled in range of 0–100%. To demonstrate preferential accumulation of the fluorescent nanogels in the inflamed paw, the enhancement ratio was calculated, which was defined as the ratio between fluorescence signal intensity (SI) of the inflamed paw and fluorescence SI of the opposite (untreated control) paw of the same animal. The region of interest (ROI) function was used to calculate the fluorescence SI using the same area of mice pawat various time points (27).

Statistics

All data are reported as mean ± standard deviation of three independent replicates. Statistical analysis was performed using Graphpad Prism Software Inc. version 5.0. Longitudinal data were analyzed using repeated-measure analysis of variance (ANOVA), where the treatment groups were considered as the within-subject factor. The analysis was followed by Tukey multiple pairwise comparisons on each day, where appropriate. P values less than 0.05 were considered statistically significant.

RESULTS

Size and Morphology of Nanogels

Formation of Zn^{2+}-coordinated complexes of PEGylated L-histidine substituted PEI (HP-PEI) and successive self-assembly of the complexes were considered as the primary step for synthesis of the nanogels. The sizes increased exponentially if the molar ratio of Zn^{2+}/N and pH increased (Fig. 2a). The optimum condition defined by the target value of 100 nm comprises the molar ratio of Zn^{2+}/N = 0.2 and

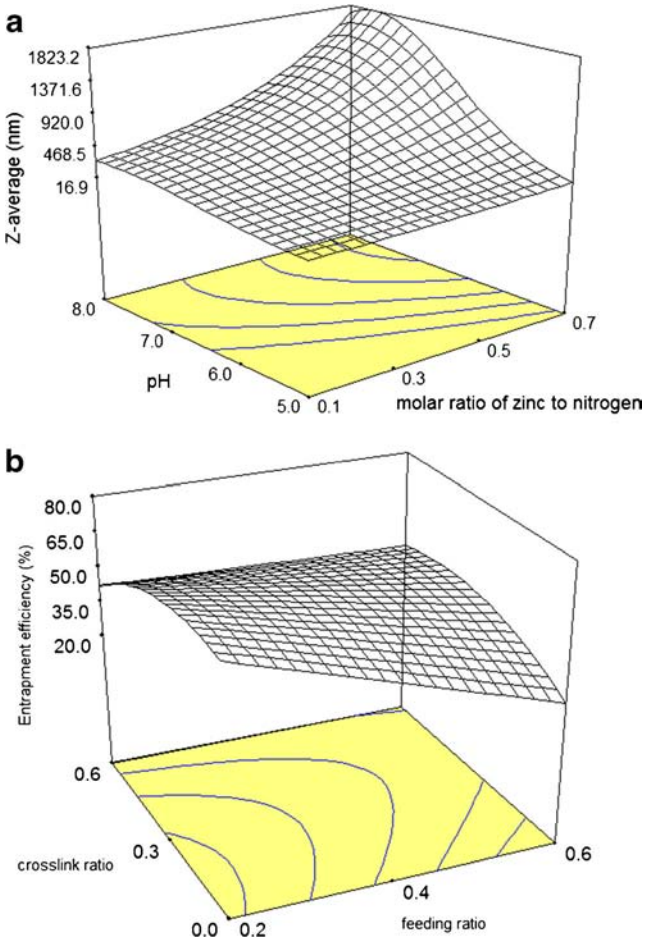

Fig. 2 (**a**) Hydrodynamic size (Z-average) of the Zn^{2+}-coordinated complexes of PEGylated, L-histidine substituted poly ethyleneimine (HP-PEI) as a function of pH and molar ratio of Zn^{2+} to the polymer nitrogen, (**b**) Entrapment efficiency (EE%) of methotrexate in the nanogels as a function of the feeding ratio and the crosslink ratio.

pH = 5.5 which resulted in the average size of 96.3 ± 42.3 nm. After crosslinking reaction, the higher crosslink ratio (CR), the smaller sizes were obtained (Table I), but after removing Zn^{2+} in the next step, the sizes increased depending on CR. The increase was more intense for the lower CR.

MTX was successfully immobilized into the nanogels following post-loading procedure. Figure 2b shows the drug loading as a function of CR and the feeding ratio (FR). Although an increase of FR led to a significant decline of entrapment efficiency (EE%) of uncrosslinked HP-PEI (EE% = 36% at FR = 0.3), it remained at high level for the nanogels synthesized at CR of 0.3 (EE% = 62% ar FR = 0.3) and 0.6 (EE% = 52% at FR = 0.3). Therefore, the optimum EE% of 62% (corresponds to the drug loading of 54%, the mass and the molar ratio of entrapped MTX to polymer equals to 1.17 *w*/*w* and 55 mol/mol) was achieved at FR = 0.3 and CR = 0.3. The drug loading was robust at different pH in range of 5–7.

MTX-loaded nanogels were homogeneous and all polydispersity index (PDI) values were less than 0.1 (Table I). Their average sizes and PDI were statistically lower than the related size parameters of the empty nanogels ($P < 0.05$ and $P < 0.01$, respectively). Moreover, the drug loaded nanogels had significantly smaller average sizes and PDI than uncrosslinked HP-PEI/MTX nanoparticles (the average size of 387 ± 105 nm and PDI of 0.21). The empty nanogels were little positively charged, but the MTX-loaded nanogels exhibited near zero values of zeta-potential.

Figure 3 shows small, uniform and round core-shell structured nanoparticles recognized by light grey cores surrounded by dark grey shells similarly for empty and MTX-loaded (FR = 0.3) nanogels synthesized at CR = 0.6.

Hemocompatibility

Figure 4a shows PEI induced a concentration-dependent hemolysis. A reduced, but still significant hemolysis was found similarly for H-PEI and HP-PEI. The nanogels showed no hemolytic effect at concentrations as high as 1 mg/ml ($P > 0.05$). Likewise, a strong erythrocyte aggregation induced by PEI and to a less extent by HP-PEI, though the aggregation disappeared completely for the nanogels (Supplementary Data 6).

Table I Intensity-Average Diameter (Z-average), Polydispersity Index (*PDI*) and Zeta-Potential of PEGylated L-histidine Substituted Poly Ethyleneimine (HP-PEI) Nanogels Following Formation of Zn^{2+} Coordinated Complex, Before and After Methotrexate (*MTX*) Loading at the Feeding Ratio of 0.3

Crosslink ratio	Condition	Z-average (nm)	Polydispersity index (PDI)	Zeta-potential[a] (mV)
0.3	Zn^{2+} coordination	190.3 ± 77.1	0.38 ± 0.04	ND[b]
0.3	Empty nanogel	247.0 ± 8.5	0.31 ± 0.02	+5.5 ± 4.1
0.3	MTX-loaded nanogel	174.0 ± 30.6	0.10 ± 0.01	0.0 ± 4.0
0.6	Zn^{2+} coordination	45.0 ± 2.8	0.12 ± 0.01	ND
0.6	Empty nanogel	190.5 ± 36.1	0.35 ± 0.03	+1.6 ± 3.2
0.6	MTX-loaded nanogel	195.0 ± 34.7	0.09 ± 0.01	−0.2 ± 5.1

Data represent mean ± SD for 3 individual experiments

[a] The measurement was made in phosphate buffered saline (10 mM phosphate salts + 0.14 M NaCl, pH 7.4)

[b] Not determined

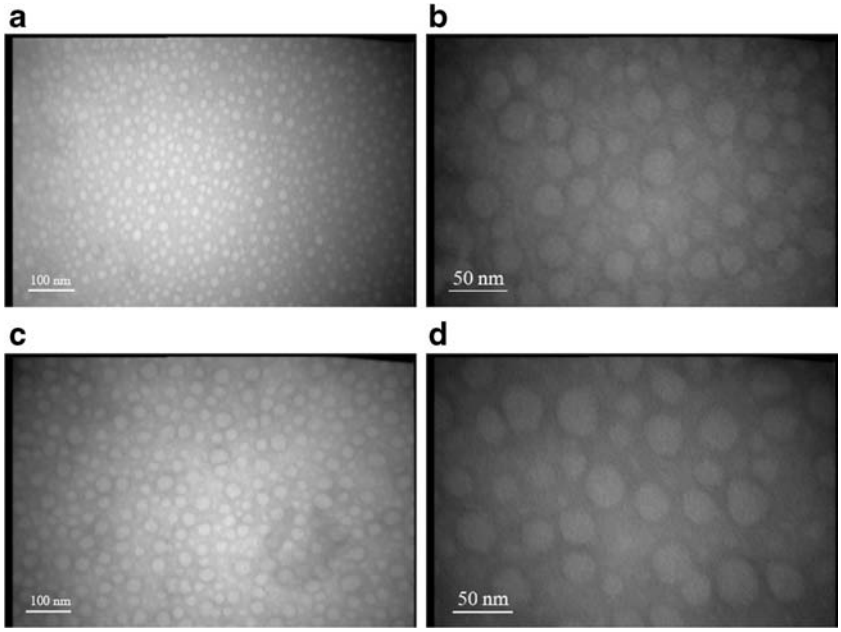

Fig. 3 Transmission electron microscopy of unloaded (**a**, **b**) and methotrexate-loaded (**c**, **d**) nanogels imaged at different magnifications.

Serum albumin aggregation may happen following the polymer exposure to blood. Figure 4b shows that PEI, H-PEI or even HP-PEI induced albumin aggregation in a concentration-dependent pattern. Interestingly, the nanogels did not show any significant aggregation at concentrations below 1 mg/ml ($P > 0.05$).

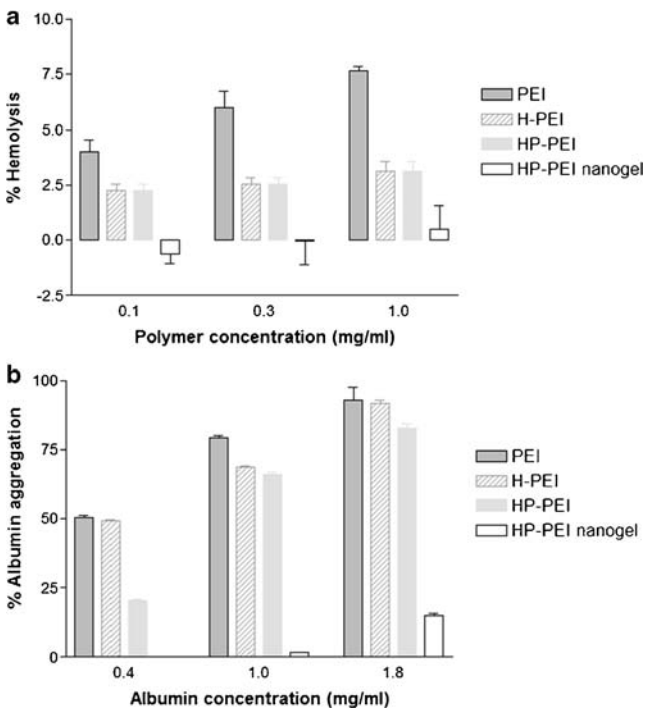

Fig. 4 Hemolysis (**a**) and albumin aggregation (**b**) of L-histidine substituted poly ethyleneimine (H-PEI), uncrosslinked PEGylated, L-histidine substituted poly ethyleneimine (HP-PEI) and HP-PEI nanogel *versus* PEI ($M_W = 10$ kDa).

Methotrexate Release and Pharmacokinetics

Prior to do the pharmacokinetic experiment, *in-vitro* drug release was determined. Figure 5 shows a prolonged release profile of the MTX-loaded nanogels if compared with free drug (first-order half-life of 2.1 h) over 24 h. Also, there was no significant burst release at early time points. It was realized from the Korsmeyer-Peppas equation that the release exponent (n) increases from 0.52 to 0.85 if 25 mM phosphate buffer (pH 7.4) is supplemented with 140 mM NaCl instead of 5% dextrose, however the rate constant (k) was similarly determined 0.1 h^{-1}.

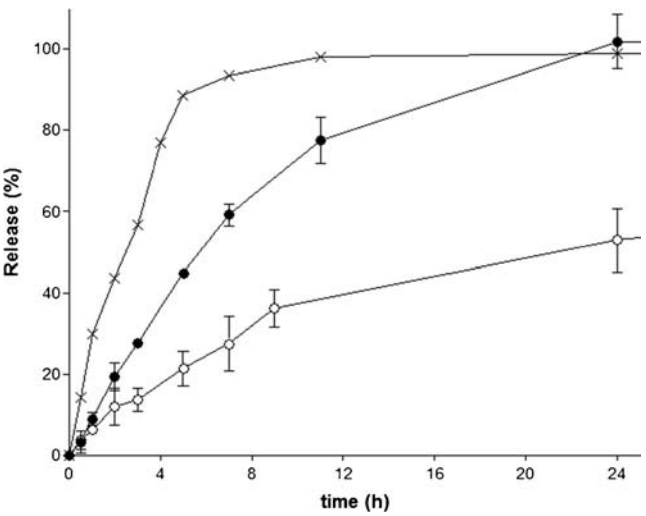

Fig. 5 *In-vitro* cumulative release of methotrexate (*MTX*) from PEGylated L-histidine substituted poly ethyleneimine (HP-PEI) nanogels in 140 mM NaCl (●) or 5% dextrose (○) supplemented 25 mM phosphate buffer (pH 7.4) in comparison to free MTX transport (×). Data represent mean ± SD for 3 independent replicates.

To investgate pharmacokinetics of MTX, first suitability of the HPLC assay method was verified in plasma samples spiked with free MTX, empty and MTX-loaded nanogels for possible interference of the resulting peaks (Supplementary Data 7). The chromatogram peaks related to MTX and timolol (internal standard) were well resolved with a corresponding AUC ratio similar to free MTX. Also, no interfering peak was found for the empty nanogels. Figure 6 shows the plasma concentrations of MTX solution declined rapidly with an effective half-life 10.7 ± 1.5 min. No drug was detected in plasma 180 min after I.V. administration. The plasma concentrations of MTX-loaded nanogel were significantly higher than free MTX at different time intervals ($P<0.0001$). A reduced clearance from the blood stream with $t_{1/2}$ of 63.3 ± 3.8 min was calculated for the MTX-loaded nanogel (Table II).

Clinical Evaluation in Collagen Induced Arthritis Mice

Mice immunized with chicken type II collagen plus CFA shares several clinical features of the disease including periarticular erythema and edema first appeared in the hind paws and weight loss. The incidence of CIA was about 90% in C57Bl/6 mice between Day 25 and Day 27. No relevant side effects (e.g., continuous weight loss, abnormal animal behavior or signs of sickness) were seen after administration of the nanogels in the preliminary safety experiment.

Figure 7a shows as early as one day after beginning the treatment with 1 mg/kg/day MTX, either as solution or loaded in nanogels, a significant reduction of paw swelling was observed ($P<0.05$), though the normal saline treated control

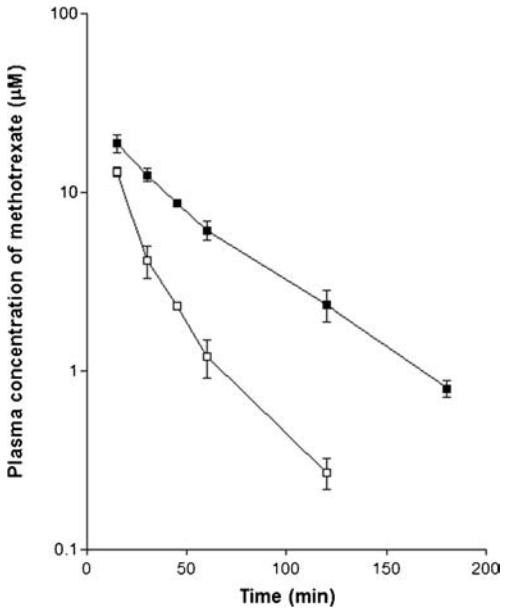

Fig. 6 Plasma concentration profile of 7 mg/kg I.V. dose of methotrexate, either as free solution (□) or loaded in the nanogels (■), in C57Bl/6 mice weighed 30.4 ± 1.0 g.

Table II Pharmacokinetic Parameters of Methotrexate Calculated After Intravenous Injection of 7 mg/kg Free Methotrexate Solution or the Drug Loaded in PEGylated L-histidine Substituted Poly Ethyleneimine (HP-PEI) Nanogel in C57Bl/6 Mice

Pharmacokinetic parameter	Free methotrexate	Methotrexate loaded HP-PEI nanogel
$AUC_{0\text{-}t}$ (μM.min)	644 ± 32	1212 ± 89
$AUC_{0\text{-}\infty}$ (μM.min)	651 ± 32	1259 ± 89
$AUMC_{0\text{-}\infty}$ (μM.min^2)	10,000 ± 1399	59,500 ± 6881
MRT (min)	15.5 ± 2.2	91.4 ± 5.5
$t_{1/2}$ (min)	10.7 ± 1.5	63.3 ± 3.8
Cl (ml/min)	0.70 ± 0.08	0.36 ± 0.06
V_{ss} (ml)	10.73 ± 1.92	32.95 ± 5.55

all Results were expressed as mean ± SD ($n = 3$)

AUC_{0-t} area under the curve from zero to 120 min, *$AUC_{0-\infty}$* area under the curve from zero to time infinity, *AUMC* area under the moment curve, *MRT* mean residence time, *$t_{1/2}$* effective half-life, *Cl* clearance, *V_{ss}* apparent volume of distribution at steady-state

did not display any retrieval. The paw swelling decreased continuously until Day 31 when no further swelling was recognized for the mice treated with MTX-loaded nanogels ($P<0.01$). Unlike MTX solution, a complete recovery happened for the mice treated with MTX-loaded nanogels since Day 31 ($P<0.01$). Besides, no significant difference was found between the mice treated with normal saline or the empty nanogels ($P>0.05$). Similar results were found if the arthritis score was considered for comparison (Fig. 7b). Unlike the normal saline treated control and the group treated with free MTX solution, the mice treated with MTX-loaded nanogels had shown a more pronounced decline of the arthritis score since Day 30 ($P<0.01$). Interestingly, no erythema or paw swelling was recognized for the CIA mice treated with MTX-loaded nanogels.

Figure 7c shows trend of the mouse weight during inspection period. A noticeable weight loss happened for all treatment groups between Day 22 and Day 27 as a sign of illness. Then, the mouse weight increased only for the group treated with MTX-loaded nanogels, yet the effect was only marginal ($P<0.1$).

Histopathological Evaluation

Figure 8 illustrates histopathological features of inflammatory responses in the CIA mice. The disease was characterized by congestion and edema in synovial membrane with prominent fat infiltration in joint space. There were foci of pannus formation with adjacent bone desorption. Also, there was chronic inflammatory cell infiltration composed of mast lymphocytes and plasma cells in synovial membrane. Few villous projections of synovial membrane with rich lympho plasma cells infiltration were noted (Fig. 8a and b). In few mice, scattered

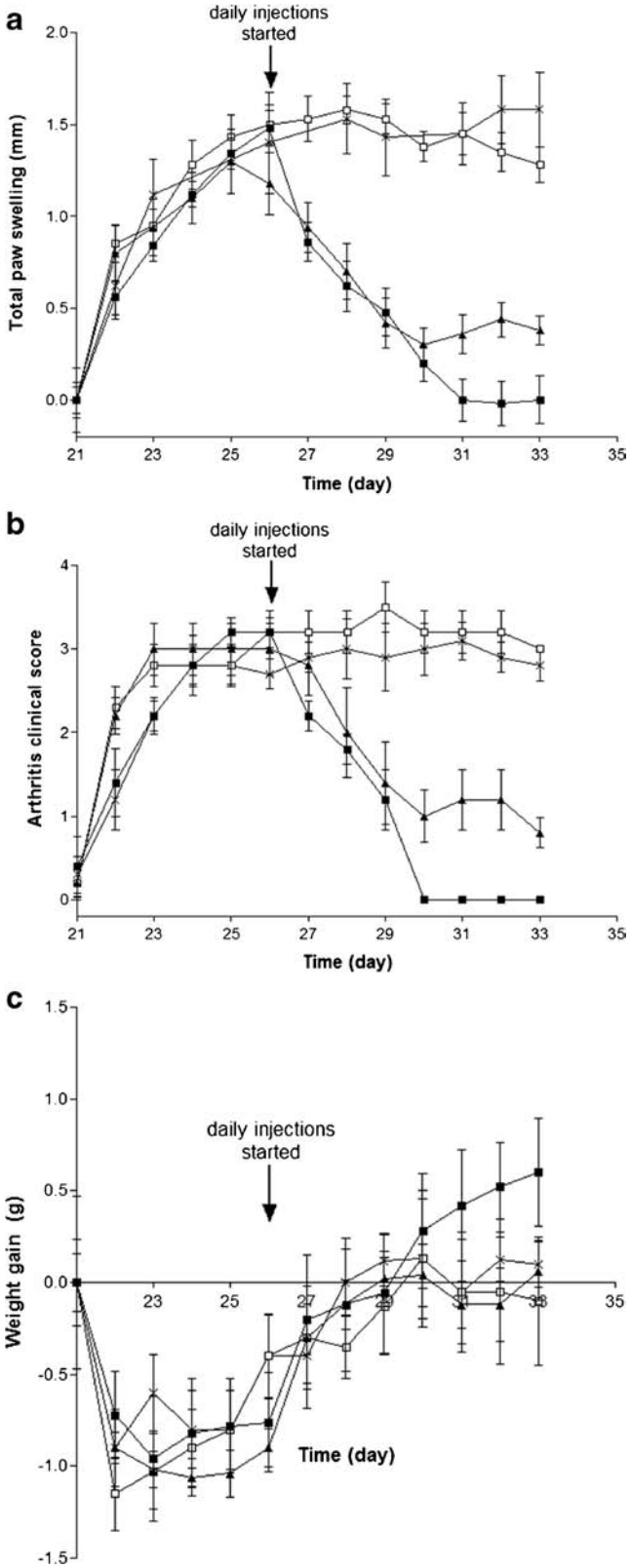

◀ **Fig. 7** Therapeutic activity of 1 mg/kg/day I.V. dose of methotrexate (*MTX*), either as free solution (▲) or loaded in the nanogels (■), in comparison to equivalent dose of 0.8 mg/kg/day empty nanogels (□) and normal saline treated control (×) started on Day 26 in collagen induced experimental arthritis. Paw swelling (**a**), arthritis clinical score (**b**) and weight gain (**c**) in the mice were noted between Day 21 and Day 33. Values are mean ± SD ($n = 5$ per each group).

infiltration of mast cells was noted in synovial membrane adjacent to site of chronic inflammation.

The inflammation infiltrate and tissue edema decreased similarly in the treatment groups compared to the control (Fig. 8c and d). These signs of joint inflammation were absent in the synovial tissue sections of the treated CIA mice with MTX-loaded nanogels (Fig. 7c). Nevertheless, only two of five sections from animals treated with free MTX solution showed still a modest joint inflammation compared with sections from untreated control mice (Fig. 8d).

In-Vivo Fluorescent Imaging Evaluation

The fluorescence intensity of the inflamed joints was considerably higher than the opposite ankle joint as after 30 min (Fig. 9), though there was no significant difference in the pre-injection fluorescence intensity in bilateral ankle joints. The average enhancement ratio of the inflamed joint was up to 1.3 ± 0.4 folds 30 min after injection of the HP-PEI nanogels, increased to 2.7 ± 0.6 folds after 1 h and then remained fairly steady until 4 h while the experiment was terminated.

DISCUSSION

Preparation of Methotrexate-Loaded Nanogels

Formation of Zn^{2+}-coordinated complexes of PEGylated L-histidine substituted PEI (HP-PEI) and the subsequent self-assembly is considered as the critical primary step for nanogel synthesis. The lyophobic complexes of Zn^{2+} and HP-PEI are stabilized by hydrophilic mPEG chains that prevent aggregation or macroscopic phase separation. Similarly, highly stable metal nanoparticles are formed in aqueous medium by reduction of the lyophobic complexes of Pd^{2+} or Pt^{2+} with diblock or graft copolymers of PEI and PEG (28). There are several factors influencing size of the coordination complexes such as pH, weight ratio of mPEG chain, type and concentration of the metal ion (29). So, size of the coordination complexes was tuned in the present study by pH and the molar ratio of Zn^{2+} (Fig. 2a). The higher ratio of Zn^{2+} resulted exponentially in the larger particles that could be explained by insufficiency of mPEG chains to stabilize the lyophobic Zn^{2+}-coordinated domains. Furthermore, the particles enlarged by increasing pH from 5.5 to 6.5. This is possibly due to a reduced protonation of the polymer backbone or a lower solubility of Zn^{2+}-coordinated complexes at more basic pH due to binding of hydroxyl ion ligands.

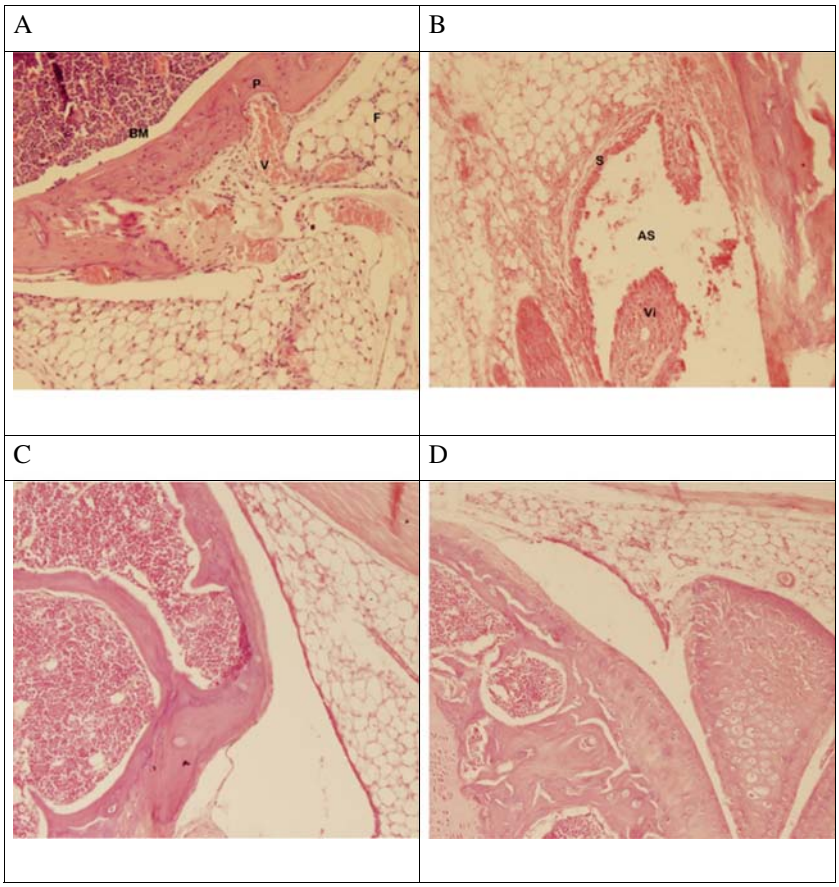

Fig. 8 Sections of the mice paw after intradermal inoculation of collagen type II in complete Freund's adjuvant on Day 33 (**a**, **b**) and after treatment with 1 mg/kg/day methotrexate-loaded nanogels (**c**) or free methotrexate solution (**d**). (hematoxylin and eosin; ×100) *S* synovium, *AS* articular space, *BM* bone marrow, *P* pannus, *V* vessel, *Vi* villous, *F* fat.

In the second step for nanogel synthesis, Zn^{2+}-coordinated complexes were served as a micellar template for chemical crosslinking reaction with DTDP, a homo-bifunctional crosslinker with a cleavable disulfide linkage (30). Following the reaction, acid dialysis was performed to prepare Zn^{2+}-free nanogel as confirmed by atomic absorption spectroscopy. Size and polydispersity of the nanogels were studied at different crosslink ratios before and after exclusion of Zn^{2+}. In line with the previous report (31), the crosslinking reaction resulted in a reduced size and polydispersity (Table I). Apart from the coordination bonds which are mainly responsible for integrity of the poly amine network, the hydrophobic interactions of imidazole side chains is also responsible for attaining small and uniform particles. After removing Zn^{2+}, which works as a condensing agent, the size increased noticeably at the nanoscale range with still narrow size distribution (Table I), so the nanogels display certain swelling property since the calculated equivalent volume might change about 50–100 times.

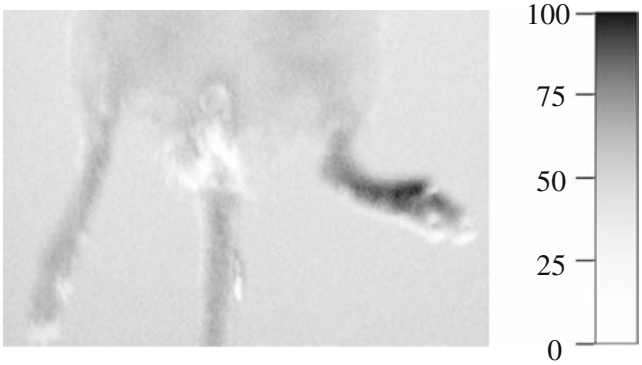

Fig. 9 *In-vivo* fluorescent imaging of inflammatory joints in the lipopolysaccharide (*LPS*) induction model. A merged fluorescent image signal of intravenously injected sulfo-cyanine 5.5 conjugated nanogels (0.21 mg/kg) with a white-light image showing specific increased fluorescence signal intensity at the affected joint after 1 h. Note the strong fluorescence signal in the LPS-treated ankle compared with the opposite control side (enhancement ratio = 2.7 ± 0.6).

Regarding to zeta-potential of the nanogels, they are classified as neutral particles with only few positive zeta-potential less than +25 mV (Table I). Large shear plane of hydrated mPEG chains around the crosslinked polyamine core may explain the reduced zeta-potential and also superior stability of the nanogels (32, 33).

The nanogels were post-loaded with MTX, a weak bicarboxylic acid with pKa values of 3.8 and 4.8. The hallow spaces of the nanogels provide free diffusion of MTX molecules and consequently results in high drug loading (Fig. 2b). However, the uncrosslinked polymer showed an attenuated entrapment efficiency (EE%) at the high level of feeding ratio that might be explained by formation of charge-neutralized

hydrophobic domains with HP-PEI that in turn prevents loading of another drug molecules. EE% of the nanogels was comparable to the previous reports on polymeric micelles (34), solid lipid nanoparticles (35), chitosan nanogel prepared by ionic gelation (36), and micellar nano-networks of PEG-*g*-PEI (19). However, it shows noticeably higher drug loading. The hydrodynamic size of nanogels decreased in DLS experiment after drug loading specially at the low crosslink ratio (Table I). It could be explained by additional physical crosslink action of MTX mainly through electrostatic interaction to the polyamine core, as similarly addressed in literature (31). Notably, the MTX-loaded nanogels exhibited zero value of zeta-potential, suggesting that negatively charged MTX molecules are effectively neutralized within the PEG corona stabilized polyamine core than being associated on the nanogel surface.

TEM experiment provides us further information regarding the micro-structure of empty and the drug-loaded nanogels. Both represent homogenous, spherical and core-shell structured particles with sizes less than 50 nm in "dry state" (Fig. 3). A slight increase of the size happens after drug loading without altering particle distribution, implying that successful loading of MTX accompanies with a modest increase of the total dehydrated mass of the nanogels.

Hemocompatibility of the Nanogels

Despite widespread applications of PEI, it demonstrates some safety problems to different extents depending on their molecular weight, charge density, structure and conformational flexibility (37). In the prelimineray study, it was shown that the nanogels unlike PEI, PEGylated or L-histidine substituted PEI did not show any general cytotoxicity after 24 h exposure to a relatively high concentration of the polymers (up to 0.3 mg/ml) (19). In the present study, about 10% hemolysis was recognized for 3 mg/ml branched PEI that is consistent with the previous report (38). Nevertheless, less hemolytic activity was associated with L-histidine substituted PEI (H-PEI) (Fig. 4a) possibly due to a lower positive charge density in physiologic pH if compared to native PEI as discussed by different authors (39). More importantly, introduction of imidazole groups into the polymer backbone would increase rigidity of the polymer that may restrict accessibility of the positive charges to the cell membrane as previously discussed by Ryser (40). Surprisingly, the nanogels unlike uncrosslinked polymers showed no hemolytic effect or no detectable disturbance of red blood cell membranes up to 1 mg/ml (Fig. 4a). Similarly, the erythrocyte aggregation disappeared completely for the nanogels (Supplementary Data 6). These observations could be more attributed to architecture of the nanogels. Although the shielding effect of mPEG shell can avoid the negative interactions with erythrocytes, PEGylation alone is not sufficient to eliminate the erythrocyte aggregation (37, 38). It seems the noticeable reduction of zeta-potential can prevent electrostatic interactions with the anionic cell membranes.

Binding of albumin to the positively charged colloidal particles and polymers is known to lead to protein aggregation following injection into blood stream (41, 42). Not only PEI but also H-PEI showed a severe aggregation after incubation with albumin (Fig. 4b). Besides, HP-PEI showed formidable aggregations; however, the nanogels were found to drastically reduce the aggregation tendency since it has been shown that crosslinked PEI is less aggregating than PEI (38). The resistance of nanogels to albumin induced aggregation could be explained by the neutral surface charge, due to presence of a PEG shell shifting the shear plane away from the particles (32, 33), or steric hindrance of decorated mPEG shell.

In-Vitro Release and Pharmacokinetics of Methotrexate-Loaded Nanogels

The poor pharmacokinetics and rapid clearance of MTX hinders the therapeutic applications in various pathophysiological conditions such as cancer and rheumatoid arthritis (4, 43). The drug release from the nanogels shows a prolonged profile over 24 h if compared to free MTX (Fig. 5), which is consistent with the previous report (44, 45). The release data eas best fitted on Korsmeyer-Peppas model showing the MTX release is swelling-controlled; i.e., the reduced drug concentration gradient over the time period is compensated to some extents by a pronounced swelling happens simultaneously upon drug release from the nanogels. Moreover, it was found that addition of 140 mM Nacl instead of 5% dextrose to 25 mM phosphate buffer (pH 7.4) increases the release exponent (n) of Korsmeyer-Peppas equation, which indicates the electrostatic attractions between carboxylate moieties of MTX molecules and polyamine core of the nanogels (retrieved after removing Zn^{2+}-chelated hydrophobic domains) plays an important role in the drug loading. Comparing the release kinetics of HP-PEI backbone in the present study with P-PEI (19), no significant change happens following histidinylation of PEI since the lower positive charge density and higher hydrophobicity of L-histidine moieties in the polymer backbone may have a counteracting contribution to the overall release of MTX.

As shown in Fig. 6, a sustained plasma concentration profile was found for the nanogel formulation after i.v. administration, whereas free MTX solution was rapidly cleared from blood stream. The corresponding MRT and $t_{1/2}$ increased about six-fold after loading in the nanogels (Table II). Similarly, Park *et al.*(46) and Kim *et al.* (47) showed a comparable superior pharmacokinetics of different MTX liposomes after single i.v. injection of the equivalent doses. The higher $t_{1/2}$ of MTX after loading in the nanogels could be explained based on the sustained release profile of MTX from the nanogels as shown in Fig. 5. The sustained drug release results in a reduced fraction of free drug in plasma, released from those of the nanogels residing in blood circulation or deposited in the peripheral tissues, which in turn decreases the drug clearance

and increases $t_{1/2}$. Likewise, Ruckmani *et al.* noted a longer $t_{1/2}$ (14.5 *vs.* 8.2 min) and MRT (23.9 than 16.0 min) for MTX-loaded SLNs than free MTX solution after intra-peritoneal injection (35). Interestingly, the nanogels provide a more sustained delivery of MTX than SLNs; however, MRT was not prolonged to a great extent, which is possibly due to a relatively high hydrophilicity of the passively loaded MTX at physiological pH; so it is suggested to modify the drug loading process through formation of a ternary complex between MTX, Zn^{2+} and polyamine core of the nanogels (this is under study now).

Clinical and Histopathological Evaluations in the CIA Model

To investigate the therapeutic action of MTX-loaded nanogels, the CIA model of RA was developed in C57Bl/6 mice (48). The model is an immunologically relevant animal model of human RA, which is accompanied by a robust T-cell and B-cell inflammation response to type II collagen and is widely used to address questions of disease pathogenesis and to validate therapeutic targets (49). In the histopathological evaluation of the CIA model, a moderate level of synovithis, cellular infiltration, cartilage degradation, pannus and villus formation were noticed (Fig. 8). These data are in line with the previous reports on a mild to moderate arthritis in C57Bl/6 mice (48, 49).

In recent years, significant efforts have been devoted to use the potentials of different drug delivery systems such as liposomes (11) and human serum albumin (HSA) (10, 50) to improve the therapeutic efficacy of MTX in RA. Williams *et al.* showed the efficacy of I.V. administered liposomal MTX in comparison to free drug solution at the equivalent dose of 1 mg/kg/day on suppression of acute inflammation in established rat antigen-induced arthritis (11). But, the liposome formulation requires development of drug-lipid conjugates for an efficient encapsulation of MTX. Wunder *et al.* demonstrated that following intra-peritoneal administration of MTX-HSA conjugate, a five-fold higher dose of free MTX is required for an equivalent efficacy in preventing the onset of arthritis in the CIA model (10). Similarly, Fiehn *et al.* demonstrated a relatively high dose of 7.5 mg/kg MTX-HSA is significantly superior than an equivalent dose of free MTX in reducing the incidence of arthritis (50). However, the use of HSA might be associated with several disadvantages such as requirement of rigorous testing for pathogens and foaming during manipulation.

In the present study, a remarkable remission of paw swelling and the clinical scores appeared 5 days after beginning the treatment with 1 mg/kg/day MTX-loaded nanogels than the equivalent dose of free drug solution (Fig. 7); Moreover, histopathological findings confirmed efficacy of the nanogel formulation (Fig. 8).

To compare the passive accumulation of the nanogels in inflamed mice paw, *in-vivo* animal imaging was used in unilateral LPS-induced arthritis in C57Bl/6 mice (Fig. 9). Unlike CIA model which develops late-onset and systemic polyarthritis following intra-dermal injection of type II collagen antigen, intra-articular injection of LPS induces transient and localized synivial inflammation, synoviocyte hyperplasia and polymorphonuclear cell infiltration (51). Although LPS model is a bacterial toxin-induced arthritis that resembles pyogenic arthritis (27) and it differs from the CIA model which is routinely used for pharmacological screening, the advantage of this model over CIA for animal imaging is that the opposite ankle joint could be used as an internal control to show preferential accumulation of the nanogels in the inflamed *vs.* normal paw, thus demonstrating the effectiveness of the nanogel. The calculated enhancement ratio in inflamed joints increased moderately to about 2.7 whitin 1 h and then remained nearly unchanged until 4 h. The enhancement ratio is more than the minimal acceptable value of 1.5 and the reported value of 2.3 for the hydrophobically modified glycol chitosan nanoparticles (52). This accumulation of the nanogels might be due to nonspecific phagocytosis by activated macrophages, or due to the nanogels localized at the interstitial space because of increased permeability and retention effect at the inflamed tissues (5).

Conclusion

Combined sustained plasma profile of MTX (Fig. 6) and preferential accumulation of the nanogels in inflamed joints (Fig. 7) is possibly responsible for the observed superior therapeutic activity of MTX-loaded nanogels in the CIA mice model that is characterized by a remarkable decline of paw edema and inflammatory infiltrates. The nanogels comprise a poly cation core stabilized by mPEG chains avoiding unfavorable interactions with human serum albumin and erythrocytes as determined in the hemocompatibility screening; however, more sophisticated analysis such as activation of complement system are required for a careful inference. Moreover, the nanogels present some suitable pharmaceutical properties such as small size and uniformity, globular structure and high drug loading capacity. Therefore, MTX-loaded nanogels can be considered to be used alone or in combination with free drug for enhancing the therapeutic index in RA, which needs more detailed and mechanistic studies.

ACKNOWLEDGMENTS AND DISCLOSURES

The authors gratefully acknowledge use of the facilities of Center for Nanotechnology in Drug Delivery, National Nanotechnology Laboratory Network and Shiraz University of Medical Sciences. Also, they would like to thank Mr. Kouhi from Central Animal Lab, Ms. Taki from Autoimmune Diseases Research Center and Ms. Abedini from Pathology Department at Khalili Hospital, Shiraz University of Medical Sciences.

Disclosure The authors declare no competing financial interests.

REFERENCES

1. Smolen JS, Steiner G. Therapeutic strategies for rheumatoid arthritis. Nat Rev Drug Discov. 2003;2(6):473–88.
2. Purcell WT, Ettinger DS. Novel antifolate drugs. Curr Oncol Rep. 2003;5(2):114–25.
3. Lee DM, Weinblatt ME. Rheumatoid arthritis. Lancet. 2001;358(9285):903–11.
4. Grim J, Chladek J, Martinkova J. Pharmacokinetics and pharmacodynamics of methotrexate in non-neoplastic diseases. Clin Pharmacokinet. 2003;42(2):139–51.
5. Abolmaali S, Tamaddon A, Dinarvand R. A review of therapeutic challenges and achievements of methotrexate delivery systems for treatment of cancer and rheumatoid arthritis. Cancer Chemother Pharmacol. 2013;71(5):1115–30.
6. Levick JR. Microvascular architecture and exchange in synovial joints. Microcirculation. 1995;2(3):217–33.
7. Koch AE, Distler O. Vasculopathy and disordered angiogenesis in selected rheumatic diseases: rheumatoid arthritis and systemic sclerosis. Arthritis Res Ther. 2007;9 Suppl 2:S3.
8. Levick JR. Hypoxia and acidosis in chronic inflammatory arthritis; relation to vascular supply and dynamic effusion pressure. J Rheumatol. 1990;17(5):579–82.
9. Nagai T, Tanaka M, Tsuneyoshi Y, Matsushita K, Sunahara N, Matsuda T, *et al.* In vitro and in vivo efficacy of a recombinant immunotoxin against folate receptor beta on the activation and proliferation of rheumatoid arthritis synovial cells. Arthritis Rheum. 2006;54(10):3126–34.
10. Wunder A, Muller-Ladner U, Stelzer EH, Funk J, Neumann E, Stehle G, *et al.* Albumin-based drug delivery as novel therapeutic approach for rheumatoid arthritis. J Immunol. 2003;170(9):4793–801.
11. Williams AS, Camilleri JP, Amos N, Williams BD. Differential effects of methotrexate and liposomally conjugated methotrexate in rat adjuvant-induced arthritis. Clin Exp Immunol. 1995;102(3):560–5.
12. Liang LS, Jackson J, Min W, Risovic V, Wasan KM, Burt HM. Methotrexate loaded poly (L-lactic acid) microspheres for intra-articular delivery of methotrexate to the joint. J Pharm Sci. 2004;93(4):943–56.
13. Oh JK, Drumright R, Siegwart DJ, Matyjaszewski K. The development of microgels/nanogels for drug delivery applications. Prog Polym Sci. 2008;33(4):448–77.
14. Akiyoshi K, Kobayashi S, Shichibe S, Mix D, Baudys M, Wan Kim S, *et al.* Self-assembled hydrogel nanoparticle of cholesterol-bearing pullulan as a carrier of protein drugs: complexation and stabilization of insulin. J Control Release. 1998;54(3):313–20.
15. Legros C, Wirotius A-L, De Pauw-Gillet M-C, Tam KC, Taton D, Lecommandoux S. Poly(2-oxazoline)-based nanogels as biocompatible pseudopolypeptide nanoparticles. Biomacromolecules. 2015;16(1):183–91.
16. Abolmaali S, Tamaddon A, Najafi H, Dinarvand R. Effect of l-Histidine substitution on Sol–Gel of transition metal coordinated poly ethyleneimine: synthesis and biochemical characterization. J Inorg Organomet Polym. 2014:1–11.
17. Park TG, Jeong JH, Kim SW. Current status of polymeric gene delivery systems. Adv Drug Deliv Rev. 2006;58(4):467–86.
18. Romberg B, Hennink W, Storm G. Sheddable coatings for long-circulating nanoparticles. Pharm Res. 2008;25(1):55–71.
19. Abolmaali S, Tamaddon A, Yousefi G, Javidnia K, Dinarvand R. Sequential optimization of methotrexate encapsulation in micellar nano-network of polyethyleneimine ionomer containing redox-sensitive cross-links. Int J Nanomedicine. 2014;9:1–16.
20. Abolmaali S, Tamaddon A, Dinarvand R. Nano-hydrogels of methoxy polyethylene glycol-grafted branched polyethyleneimine via biodegradable cross-linking of Zn2 + -ionomer micelle template. J Nanopart Res. 2013;15(12):1–21.
21. Kim JO, Sahay G, Kabanov AV, Bronich TK. Polymeric micelles with ionic cores containing biodegradable cross-links for delivery of chemotherapeutic agents. Biomacromolecules. 2010;11(4):919–26.
22. Korsmeyer RW, Gurny R, Doelker E, Buri P, Peppas NA. Mechanisms of solute release from porous hydrophilic polymers. Int J Pharm. 1983;15(1):25–35.
23. Parnham MJ, Wetzig H. Toxicity screening of liposomes. Chem Phys Lipids. 1993;64(1–3):263–74.
24. Cerda-Cristerna BI, Flores H, Pozos-Guillen A, Perez E, Sevrin C, Grandfils C. Hemocompatibility assessment of poly(2-dimethylamino ethylmethacrylate) (PDMAEMA)-based polymers. J Control Release: Off J Control Release Soc. 2011;153(3):269–77.
25. Holder DJ, Hsuan F, Dixit R, Soper K. A method for estimating and testing area under the curve in serial sacrifice, batch, and complete data designs. J Biopharm Stat. 1999;9(3):451–64.
26. Bevaart L, Vervoordeldonk M, Tak P. Collagen-induced arthritis in mice. In: Proetzel G, Wiles MV, editors. Mouse models for drug discovery: Humana Press; 2010. p. 181–92.
27. Chen W-T, Mahmood U, Weissleder R, Tung C-H. Arthritis imaging using a near-infrared fluorescence folate-targeted probe. Arthritis Res Ther. 2005;7(2):1–8.
28. Bronstein LM, Sidorov SN, Gourkova AY, Valetsky PM, Hartmann J, Breulmann M, *et al.* Interaction of metal compounds with 'double-hydrophilic' block copolymers in aqueous medium and metal colloid formation. Inorg Chim Acta. 1998;280(1–2):348–54.
29. Solomatin SV, Bronich TK, Bargar TW, Eisenberg A, Kabanov VA, Kabanov AV. Environmentally responsive nanoparticles from block ionomer complexes: effects of pH and ionic strength. Langmuir. 2003;19(19):8069–76.
30. Liu J, Detrembleur C, Hurtgen M, Debuigne A, De Pauw-Gillet M-C, Mornet S, *et al.* Reversibly crosslinked thermo- and redox-responsive nanogels for controlled drug release. Polym Chem. 2014;5(1):77–88.
31. Kim JO, Kabanov AV, Bronich TK. Polymer micelles with cross-linked polyanion core for delivery of a cationic drug doxorubicin. J Control Release: Off J Control Release Soc. 2009;138(3):197–204.
32. Vinogradov SV, Bronich TK, Kabanov AV. Nanosized cationic hydrogels for drug delivery: preparation, properties and interactions with cells. Adv Drug Deliv Rev. 2002;54(1):135–47.
33. Vinogradov SV, Kabanov AV. Synthesis of nanogel carriers for delivery of active phosphorylated nucleoside analogues. Polymer Prepr. 2004;228(Pt 2):296.
34. Jeong Y, Seo D, Kim D, Choi C, Jang MJ, Nah JW, *et al.* Methotrexate-incorporated polymeric micelles composed of methoxy poly (ethyleneglycol)-grafted chitosan. Macromol Res. 2009;17(7):538–43.
35. Ruckmani K, Sivakumar M, Ganeshkumar PA. Methotrexate loaded solid lipid nanoparticles (SLN) for effective treatment of carcinoma. J Nanosci Nanotechnol. 2006;6(9–10):2991–5.
36. Azadi A, Hamidi M, Khoshayand M-R, Amini M, Rouini M-R. Preparation and optimization of surface-treated methotrexate-loaded nanogels intended for brain delivery. Carbohydr Polym. 2012;90(1):462–71.
37. Petersen H, Fechner PM, Martin AL, Kunath K, Stolnik S, Roberts CJ, *et al.* Polyethylenimine-graft-poly(ethylene glycol) copolymers: influence of copolymer block structure on DNA complexation and biological activities as gene delivery system. Bioconjug Chem. 2002;13(4):845–54.
38. Neu M, Sitterberg J, Bakowsky U, Kissel T. Stabilized nanocarriers for plasmids based upon cross-linked poly (ethylene imine). Biomacromolecules. 2006;7(12):3428–38.

39. Fischer D, Li Y, Ahlemeyer B, Krieglstein J, Kissel T. In vitro cytotoxicity testing of polycations: influence of polymer structure on cell viability and hemolysis. Biomaterials. 2003;24(7):1121–31.
40. Ryser HJ. A membrane effect of basic polymers dependent on molecular size. Nature. 1967;215(5104):934–6.
41. Rezwan K, Meier LP, Rezwan M, Vörös J, Textor M, Gauckler LJ. Bovine serum albumin adsorption onto colloidal Al2O3 particles: a new model based on zeta potential and UV − Vis measurements. Langmuir. 2004;20(23):10055–61.
42. Dobrovolskaia MA, Patri AK, Zheng J, Clogston JD, Ayub N, Aggarwal P, *et al.* Interaction of colloidal gold nanoparticles with human blood: effects on particle size and analysis of plasma protein binding profiles. Nanomedicine: Nanotechnol Biol Med. 2009;5(2):106–17.
43. Rau R, Herborn G. Benefit and risk of methotrexate treatment in rheumatoid arthritis. Clin Exp Rheumatol. 2004;22(5 Suppl 35):S83–94.
44. Ji J, Wu D, Liu L, Chen J, Xu Y. Preparation, evaluation, and in vitro release of folic acid conjugated O-carboxymethyl chitosan nanoparticles loaded with methotrexate. J Appl Polym Sci. 2012;125 SUPPL 2:E208–15.
45. Kohler N, Sun C, Wang J, Zhang MQ. Methotrexate-modified superparamagnetic nanoparticles and their intracellular uptake into human cancer cells. Langmuir. 2005;21(19):8858–64.
46. Park JM, Ahn B-N, Yoon EJ, Lee MG, Shim C-K, Kim C-K. The pharmacokinetics of methotrexate after intravenous administration of methotrexate-loaded proliposomes to rats. Biopharm Drug Dispos. 1994;15(5):391–407.
47. Kim MM, Lee SH, Lee MG, Hwang SJ, Kim C-K. Pharmacokinetics of methotrexate after intravenous and intramuscular injection of methotrexate-bearing positively charged liposomes to rats. Biopharm Drug Dispos. 1995;16(4):279–93.
48. Inglis J, Criado G, Medghalchi M, Andrews M, Sandison A, Feldmann M, *et al.* Collagen-induced arthritis in C57BL/6 mice is associated with a robust and sustained T-cell response to type II collagen. Arthritis Res Ther. 2007;9(5):1–8.
49. Campbell IK, Hamilton JA, Wicks IP. Collagen-induced arthritis in C57BL/6 (H-2b) mice: new insights into an important disease model of rheumatoid arthritis. Eur J Immunol. 2000;30(6):1568–75.
50. Fiehn C, Kratz F, Sass G, Müller-Ladner U, Neumann E. Targeted drug delivery by in vivo coupling to endogenous albumin: An albumin-binding prodrug of methotrexate (MTX) is better than MTX in the treatment of murine collagen-induced arthritis. Ann Rheum Dis. 2008;67(8):1188–91.
51. Hollingsworth JW, Atkins E. Synovial inflammatory response to bacterial endotoxin. Yale J Biol Med. 1965;38(3):241–56.
52. Park KS, Kang JH, Sa KH, Koo HB, Cho HJ, Nam EJ, *et al.* In vivo quantitative measurement of arthritis activity based on hydrophobically modified glycol chitosan in inflammatory arthritis: more active than passive accumulation. Mol Imaging. 2012;11(5):389–400.